SCIENCE CHINA
Physics, Mechanics & Astronomy

•Article•

June 2019 Vol. 62 No. 6: 064711
https://doi.org/10.1007/s11433-018-9318-4

Effects of dimensional wall temperature on velocity-temperature correlations in supersonic turbulent channel flow of thermally perfect gas

XiaoPing Chen[1], XinLiang Li[2,3*], and ZuChao Zhu[1]

[1] *Key Laboratory of Fluid Transmission Technology of Zhejiang Province, Zhejiang Sci-Tech University, Hangzhou 310018, China;*
[2] *Key Laboratory of High Temperature Gas Dynamics, Institute of Mechanics, Chinese Academy of Sciences, Beijing 100190, China;*
[3] *School of Engineering Science, University of Chinese Academy of Sciences, Beijing 100049, China*

Received July 25, 2018; accepted October 30, 2018; published online January 25, 2019

Direct numerical simulations of temporally evolving supersonic turbulent channel flows of thermally perfect gas are conducted at Mach number 3.0 and Reynolds number 4800 for various values of the dimensional wall temperature to study the influence of the latter on the velocity-temperature correlations. The results show that in a fully developed turbulent channel flow, as the dimensional wall temperature increases, there is little change in the mean velocity, but the mean temperature decreases. The mean temperature is found to be a quadratic function of the mean velocity, the curvature of which increases with increasing dimensional wall temperature. The concept of "recovery enthalpy" provides a connection between the mean velocity and the mean temperature, and is independent of dimensional wall temperature. The right tails of probability density function of the streamwise velocity fluctuation grows with increasing dimensional wall temperature. The dimensional wall temperature does not have a significant influence on the Reynolds analogy factor or strong Reynolds analogy (SRA). The modifications of SRA by Huang et al. and Zhang et al. provide reasonably good results, which are better than those of the modifications by Cebeci and Smith and by Rubesin.

direct numerical simulation, velocity-temperature correlation, supersonic flow, channel flow, thermally perfect gas, strong Reynolds analogy

PACS number(s): 47.27.ek, 47.27.nd, 47.40.Ki

Citation: X. P. Chen, X. L. Li, and Z. C. Zhu, Effects of dimensional wall temperature on velocity-temperature correlations in supersonic turbulent channel flow of thermally perfect gas, Sci. China-Phys. Mech. Astron. **62**, 064711 (2019), https://doi.org/10.1007/s11433-018-9318-4

1 Introduction

Supersonic turbulent channel flows are of great importance in engineering applications and gas dynamics. In the study of such flows, an important role is played by velocity-temperature correlations (VTC), which are of particular significance for investigations of the effect of strong wall heating on the large-scale structure of the turbulence and its contribution to heat transfer [1,2]. VTC can be derived at three different levels: from the Reynolds analogy between mean wall friction and temperature variations [3-6], from the Crocco-Busemann relation [7,8] between mean velocity and temperature, and from the strong Reynolds analogy (SRA) concerning turbulent stresses and turbulent heat fluxes [9,10].

There have been many studies focusing on the VTC for supersonic flows, including wall temperature effects. Most previous studies have considered calorically perfect gas. For

*Corresponding author (email: lixl@imech.ac.cn)

example, the Reynolds analogy was first presented by Reynolds [11] in the context of incompressible flow on the basis of the similarity between the Reynolds-averaged momentum and energy equations. Busemann [7] and Crocco [8] independently obtained a relation for compressible laminar boundary layers by assuming unit Prandtl number. Their derivations of this Crocco-Busemann relation were then extended to turbulent boundary layers by van Driest [12], and it was found that the mean temperature is a quadratic function of the mean velocity. Subsequently, based on several assumptions, including neglect of turbulent dissipation and pressure-strain terms, Walz [13] derived a modified Crocco-Busemann relation. Theories analysis [14], experimental measurements [15-19] and direct numerical simulation (DNS) [20-25] have demonstrated the validity of Walz's equation for adiabatic boundary layers. Duan et al. [24] carried out DNS of a supersonic boundary layer with different wall temperature, and found deviations from the quadratic dependence of mean temperature on mean velocity as the wall temperature decreased (and thus wall heat flux increased). Zhang et al. [26] derived a generalized Reynolds analogy by introducing a general recovery factor, which overcomes the limitations of Walz's equation in the presence of nonadiabatic wall. Moreover, Duan and Martín [27] introduced a nondimensional "recovery enthalpy" to remove the dependence of Walz's equation on thermal and chemical models.

SRA, introduced by Morkovin [9], concerns the relationship between velocity and temperature fluctuations. Three main relations based on SRA will be discussed in the present study. Two of them predict full anticorrelation between streamwise velocity and temperature $R_{u''T''} = -1$ and a constant turbulent Prandtl number $Pr_t = 1$. However, these predictions have been found to be in quite strong disagreement with experimental results for supersonic adiabatic boundary layers, which give values of $-R_{u''T''} \approx 0.5$-0.6 and $Pr_t \approx 0.7$-0.8 [10,22,28]. Moreover, non-negligible total temperature fluctuations exist, violating one of Morkovin's preconditions. These inconsistencies are even more pronounced for isothermal-wall boundary conditions in developing boundary layer [23,24,29] and in fully developed channel flows [2,30,31], for which $R_{u''T''}$ is not only far from unity but also positive. To overcome this defect, several modified SRAs have been proposed to take into account surface heat flux, such as ESRA of Cebeci and Smith [32], GSRA of Gaviglio [29], RSRA of Rubesin [33], and HSRA of Huang et al. [30]. HSRA agrees best with the results of DNS for different wall temperature and flow situations [22,23,34-37]. Duan and Martín [27] noted that HSRA was derived assuming calorically perfect gas, and proposed a generalized form (GHSRA) with this assumption removed.

For supersonic flows, the isothermal wall condition is widely employed. However, for engineering applications, it is often necessary to take account of the effects of varying wall temperature. If the temperature near the wall is very high, and a new thermodynamic environment may be established compared with that at lower temperatures. In particular, when the temperature is above 500 K, specific heats become a function of temperature, in which is called thermally perfect gas (TPG) [38-40]. Chen et al. [41,42] studied the effects of TPG on the turbulence statistics and energy transfer, based on the DNS data for a high-temperature supersonic turbulent channel flow. They found that the turbulent flow field is significantly related to the dimensional wall temperature. However, no definitive results have been reported on the influence of the dimensional wall temperature on the VTC in supersonic turbulent channel flow (STCF) of TPG. Therefore, the main purpose of the present study is to investigate the influence of dimensional wall temperature on the VTC under these conditions.

The remainder of the paper is organized as follows. The governing equations and details of the DNS are given in sects. 2 and 3, respectively. Sect. 4 presents the results of the DNS, together with a discussion. Finally, we summarize our findings in sect. 5.

2 Governing equations

The governing equations are the time-dependent three dimensional Navier-Stokes equations in nondimensional form. The governing equations for mass, momentum, and energy conservation, respectively, are as follows:

$$\frac{\partial \rho}{\partial t} + \frac{\partial}{\partial x_j}(\rho \boldsymbol{u}_j) = 0, \tag{1}$$

$$\frac{\partial (\rho \boldsymbol{u}_i)}{\partial t} + \frac{\partial}{\partial x_j}\left(\rho \boldsymbol{u}_i \boldsymbol{u}_j + p\boldsymbol{\delta}_{ij} - \frac{1}{Re}\boldsymbol{\sigma}_{ij}\right) = \rho \boldsymbol{f}_i, \tag{2}$$

$$\frac{\partial E}{\partial t} + \frac{\partial}{\partial x_j}\left[(E+p)\boldsymbol{u}_j - \frac{1}{Re}\left(\boldsymbol{u}_i \boldsymbol{\sigma}_{ij} + q_j\right)\right] = \rho \boldsymbol{f}_i \boldsymbol{u}_i, \tag{3}$$

where ρ, p, T and $\boldsymbol{u}_j$ are the nondimensionalized density, pressure, temperature and velocity vector, respectively. The velocity is nondimensionlized by its free-stream values, and these thermaldynamic quantities (density, pressure and temperature) are nondimensionlized by their wall values. $\boldsymbol{f}_i$ is the body force vector and is non-zero only for i=1. Re is the Reynolds number. The pressure p, total energy E, shear stress tensor $\boldsymbol{\sigma}_{ij}$ and conductive heat flux q_j are given by

$$p = \frac{\rho T}{\gamma Ma^2}, \tag{4}$$

$$E = \rho\left(C_V T + \frac{1}{2}u_i \boldsymbol{u}_i\right), \tag{5}$$

$$\boldsymbol{\sigma}_{ij}=\mu\left(\frac{\partial \boldsymbol{u}_i}{\partial x_j}+\frac{\partial \boldsymbol{u}_j}{\partial x_i}\right)-\frac{2}{3}\mu\frac{\partial u_k}{\partial x_k}\boldsymbol{\delta}_{ij}, \tag{6}$$

$$q_j=\frac{C_{\mathrm{p}}\mu}{Pr}\frac{\partial T}{\partial x_j}, \tag{7}$$

where $\boldsymbol{\delta}_{ij}$ is the Kronecker tensor, Ma is the Mach number, Pr is the Prandtl number, μ is the viscosity (calculated by the Sutherland's law, $\mu=T^{3/2}\left(1+110.4/T_{\mathrm{w}}^{**}\right)/\left(T+110.4/T_{\mathrm{w}}^{**}\right)$, double asterisks ** indicates dimensional flow variables). γ is the specific heat ratio, and C_{V} and C_{p} are the specific heat at constant volume and pressure. The gas is assumed to be the pure air consisting of molecular oxygen (O_2) and molecular nitrogen (N_2). Its specific heat is the sum of translational, rotational, and vibrational specific heats

$$C_{\mathrm{V}}=C_{\mathrm{V,tr}}+C_{\mathrm{V,r}}+C_{\mathrm{V,v}}, \tag{8}$$

$$C_{\mathrm{p}}=C_{\mathrm{V}}+R, \tag{9}$$

$$\gamma=C_{\mathrm{p}}/C_{\mathrm{V}}, \tag{10}$$

where R is the nondimensionalized gas constant. The translational, rotational, and vibrational specific heats at constant volume can be calculated respectively as [38-42]:

$$C_{\mathrm{V,tr}}=\frac{3}{2}R^{**}\frac{T_{\mathrm{w}}^{**}}{u_{\mathrm{b}}^{**2}}, \tag{11}$$

$$C_{\mathrm{V,r}}=R^{**}\frac{T_{\mathrm{w}}^{**}}{u_{\mathrm{b}}^{**2}}, \tag{12}$$

$$C_{\mathrm{V,v}}=\left(\frac{\theta^{**}}{T^{**}}\right)^2\frac{\exp(\theta^{**}/T^{**})}{\left[\exp(\theta^{**}/T^{**})-1\right]^2}\frac{T_{\mathrm{w}}^{**}}{u_{\mathrm{b}}^{**2}}, \tag{13}$$

where θ is the characteristic vibrational temperature. Bulk and wall conditions are indicated by subscript b and w denote, respectively.

3 Descriptions of the DNS

Five DNS of temporally evolving STCF, with dimensional wall temperatures ranging from 149.075 to 1788.90 K, are conducted at Mach number 3.0 and Reynolds number 4880. The Mach number, $Ma=u_{\mathrm{b}}/c_{\mathrm{w}}$, is based on the bulk velocity and sound speed at the isothermal wall, and the Reynolds number, $Re=\rho_{\mathrm{w}}u_{\mathrm{b}}H/\mu_{\mathrm{w}}$, is based on the bulk density, bulk velocity, channel half-width, and viscosity at the isothermal wall. The flow and computational parameters are given in Table 1. The Prandtl number Pr and wall temperature T_{w} are 0.7 and 1.0, respectively.

The DNS results are generated using the code developed by Chen et al. [41,42]. The numerical code has been developed from code for calorically perfect gas (Li et al. [34,43-47], OPENCFD). OPENCFD has been proven to be very useful for a wide range of supersonic and hypersonic turbulent flows, including supersonic turbulent channel flows. The Navier-Stokes equations, shown in sect. 2, are solved by Van-Leer flux vector splitting, and the 7th weighted essentially non-oscillatory scheme [48] is used to discrete the convection terms. The viscous terms are approximated with an 8th central difference scheme. A 3rd Runge-Kutta method is used for time integration. Periodic boundary conditions are adopted in the streamwise and spanwise directions for computational efficiency. On the wall boundaries, nonslip conditions are used for the velocity, and the wall temperature is kept isothermal.

The computational domain and grid parameters are given in Table 2. The computational domain size is $L_x\times L_y\times L_z=4\pi H\times 2H\times 4\pi H/3$ in the stream-wise x, wall-normal y and span-wise z directions, respectively. The number of grid points is $n_x\times n_y\times n_z=571\times 261\times 251$ with a hyperbolic-tangent-type stretching in the wall-normal direction. The grid spacings in the three directions are shown in Table 2.

Averages are performed over the homogeneous directions (x and z) and time (t). This averaging process implies that any partial derivative of a variable quantity in the wall-normal direction is equivalent to a total derivative. Let us introduce the notation used in the equations that follow: $\langle\cdot\rangle$ and $\{\cdot\}$ denote ensemble and Favre averages, respectively. Turbulent fluctuations with respect to the Reynolds and Favre averages are indicated by single ($'$) and double ($''$) primes, respectively.

Isothermal walls lead to mean property variations that are qualitatively different from those found in adiabatic wall boundary layers [3], since they allow the heat generated by dissipation to be transformed out of the channel. Steep near-wall mean gradients are very important attributes of isothermal wall flow. Some of the quantities, which are specific

Table 1 Flow and computational parameters for different dimensional wall temperature

Cases	T_{w}^{*} (K)	Ma	Re	Pr	T_{w}
WT1	149.075	3.0	4880	0.7	1.0
WT2	298.15	3.0	4880	0.7	1.0
WT3	596.30	3.0	4880	0.7	1.0
WT4	1192.6	3.0	4880	0.7	1.0
WT5	1788.9	3.0	4880	0.7	1.0

to the present non-adiabatic boundary layer, are investigated here. The friction Mach number, $Ma_\tau = u_\tau / c_w$, is based on the wall sound speed and friction velocity ($u_\tau = \sqrt{\tau_w / \rho_w}$, $\tau_w = \sqrt{\mu_w (\partial \langle u \rangle / \partial y)\big|_w}$). The friction Reynolds number, $Re_\tau = \rho_w u_\tau H / \mu_w$, is based on the channel half-width and the wall friction velocity. A nondimensional heat flux, $B_q = -q_w / \rho_w C_{pw} u_\tau$ (where the wall heat flux is $q_w = C_{pw} \mu_w / Pr (\partial \langle T \rangle / \partial y)\big|_w$), is another "inner layer" parameter and, together with Ma_τ is assumed to uniquely determine the compressible law of the wall [3]. A summary of the values of these and other time-averaged data for different dimensional wall temperature conditions is given in Table 3.

4 DNS results and discussions

4.1 Velocity and temperature analysis

To represent the degree of vibrational energy excitation, we adopt the "vibrational energy excited degree [49]," defined as the ratio of vibrational specific heat at constant volume to the sum of the other two specific heats at constant volume:

$$\phi_{C_V} = \frac{\langle C_{V,v} \rangle}{\langle C_{V,tr} \rangle + \langle C_{V,r} \rangle}. \tag{14}$$

Note that ϕ_{C_V} has an strong temperature dependence, increasing significantly with increasing dimensional wall temperature, as shown in Figure 1. For low dimensional wall temperature condition WT1, whose flow field is very close to that of calorically perfect gas, the contribution of vibrational energy is very small with a peak value of ϕ_{C_V} of just 0.009. However, for WT3, for which ϕ_{C_V} is greater than 0.1 in most regions of the channel, the vibrational energy becomes important. When the dimensional wall temperature increases to 1788.30 K (WT5), the peak value of ϕ_{C_V} reaches 0.376 indicating that the vibrational energy has become fully excited.

Figure 2(a) and (b) show the mean velocity $\{u\}$ and mean temperature $\{T\}$ in the wall-normal direction, respectively. It can be seen that $\{u\}$ is only slightly affected by the dimensional wall temperature, whereas $\{T\}$ decreases with increasing dimensional wall temperature. The main reason for this is that the excited vibrational energy leads to a more significant transformation of more significant transform of kinetic energy to internal energy.

Figure 3 shows the van Driest transformed velocity $\langle u \rangle^+_{vd}$ versus wall scaling y^+, which are defined as:

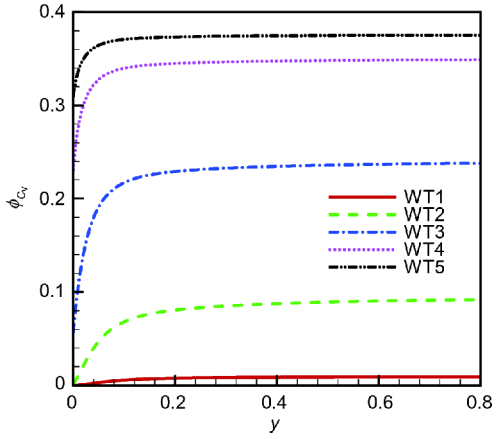

Figure 1 (Color online) Distribution of vibrational energy excited degree for different dimensional wall temperature.

Table 2 Grid resolution and domain size for different dimensional wall temperature

Cases	L_x/H	L_y/H	L_z/H	n_x	n_y	n_z	Δx^+	Δy^+_w	Δy^+_{max}	Δz^+
WT1	4π	2	4π/3	571	261	251	10.12	0.243	8.97	7.676
WT2	4π	2	4π/3	571	261	251	9.763	0.230	8.65	7.403
WT3	4π	2	4π/3	571	261	251	9.419	0.226	8.35	7.149
WT4	4π	2	4π/3	571	261	251	9.248	0.222	8.19	7.014
WT5	4π	2	4π/3	571	261	251	9.061	0.218	8.03	6.871

Table 3 Time-averaged parameters for different dimensional wall temperature

Cases	Ma_τ	Re_τ	$-B_q$	$\langle \rho_w \rangle$	$\langle \rho_c \rangle$	$\langle T_c \rangle$	$\langle \mu_c \rangle$	$\langle \gamma_w \rangle$	$\langle \gamma_c \rangle$
WT1	0.115	460.52	0.1455	2.444	0.948	2.550	2.154	1.400	1.396
WT2	0.118	443.59	0.1344	2.317	0.952	2.380	1.829	1.399	1.366
WT3	0.123	428.25	0.1282	2.142	0.955	2.136	1.598	1.378	1.323
WT4	0.127	420.24	0.1193	2.039	0.957	2.069	1.503	1.325	1.296
WT5	0.128	411.74	0.0952	1.984	0.959	2.029	1.437	1.305	1.291

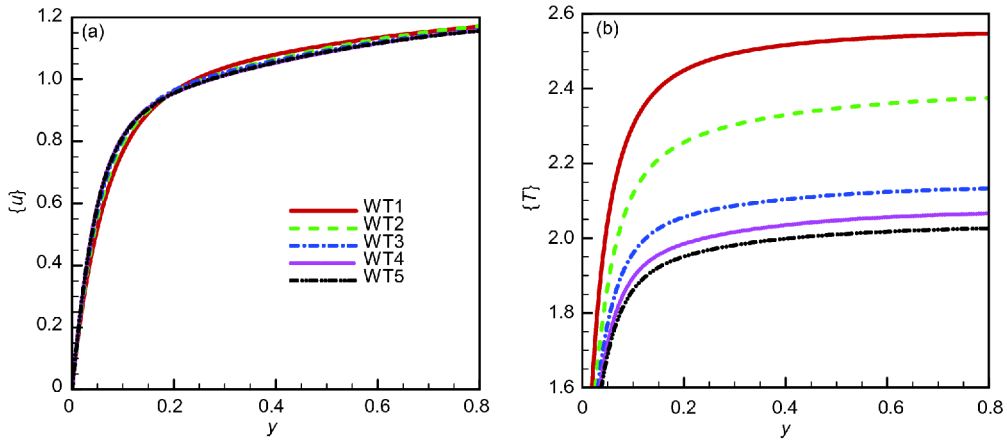

Figure 2 (Color online) Distributions of mean velocity (a) and mean temperature (b) for different dimensional wall temperature.

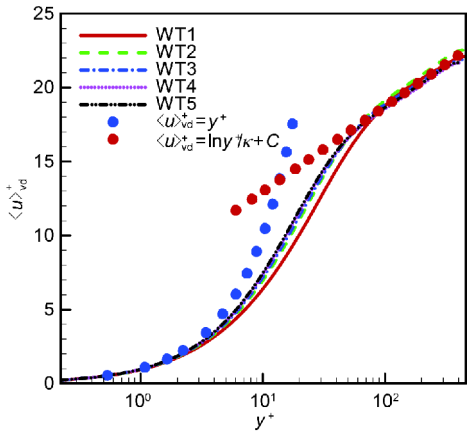

Figure 3 (Color online) Distribution of van Driest transformed velocity.

$$\langle u\rangle_{\mathrm{vd}}^{+}=\int_{0}^{\langle u\rangle^{+}}\sqrt{\frac{\langle\rho\rangle}{\langle\rho_{\mathrm{w}}\rangle}}\,d\langle u\rangle^{+},\quad \langle u\rangle^{+}=\frac{\langle u\rangle}{u_{\tau}},\tag{15}$$

$$y^{+}=y\frac{\rho_{\mathrm{w}}u_{\tau}}{\mu_{\mathrm{w}}}.\tag{16}$$

Note that the profiles of the van Driest transformed velocity for different dimensional wall temperature conditions collapses to the incompressible log law

$$\langle u\rangle_{\mathrm{vd}}^{+}=\frac{1}{\kappa}\ln y^{+}+C,\tag{17}$$

with Kármán constant κ similar to the incompressible value 0.41. However, the logarithmic curve coefficient C is greater than 5.5, which is different from that of incompressible flow [3].

The root mean square (RMS) velocity fluctuations provide an appropriate measure of the turbulent intensity. RMS velocity fluctuation, defined as $u''_{\mathrm{rms}}=\langle u''u''\rangle^{1/2}$ (and similarly for v''_{rms} and w''_{rms}), is often used to quantify the turbulent intensity. These fluctuations, normalized by conventional wall variables (defined in terms of the mean density, viscosity, and shear stress at the wall), are shown in Figure 4(a), from which it can be seen that there are clear variations with dimensional wall temperature. For example, the peak value increases with increasing dimensional wall temperature, and the position of the peak shifts further away from the wall, especially for u''_{rms}. In addition, Figure 4(b) shows the RMS temperature fluctuation ($T''_{\mathrm{rms}}=\sqrt{T''^{2}}$) versus wall scaling ($y^{+}=y\rho_{\mathrm{w}}u_{\tau}/\mu_{\mathrm{w}}$). Fairly large temperature fluctuations are found for all cases, especially close to the wall. The magnitude of $T''_{\mathrm{rms}}/\{T\}$ increases with decreasing dimensional wall temperature, and the maximum values shift further away from the wall.

Figure 5(a) and (b) show the turbulent Mach number Ma_{t} and RMS Mach number fluctuation Ma'_{rms}, respectively. The turbulent Mach number, defined as the ratio of the RMS velocity fluctuation to the mean sound speed, $Ma_{\mathrm{t}}=\sqrt{u''_{j}{}^{2}}/\{c\}$($c=\sqrt{\gamma RT}/Ma$ is the sound speed), is an indicator of the significance of compressibility effects. According to ref. [10], Ma_{t} has a threshold of 0.3, above which compressibility effects become important for turbulent behavior. It can be seen from Figure 5(a) that there are some regions in the flow where Ma_{t} is greater than 0.3. The magnitudes of Ma_{t} increases with increasing dimensional wall temperature close to the wall, which is due mainly to the difference in mean sound speed in this region. The peak value of Ma_{t} is about 0.410 for WT5, compared with a peak value of 0.356 for WT1. In addition, it is commonly believed that RMS Mach number fluctuation, $Ma'_{\mathrm{rms}}=\sqrt{(u/c)'^{2}}$, exhibits a similar trend to Ma_{t}. This conclusion has been confirmed for compressible turbulent channel flows by Coleman et al. [35] and hypersonic turbulent boundary layers by Duan et al. [24,25,27]. Coleman et al. [35] also reported

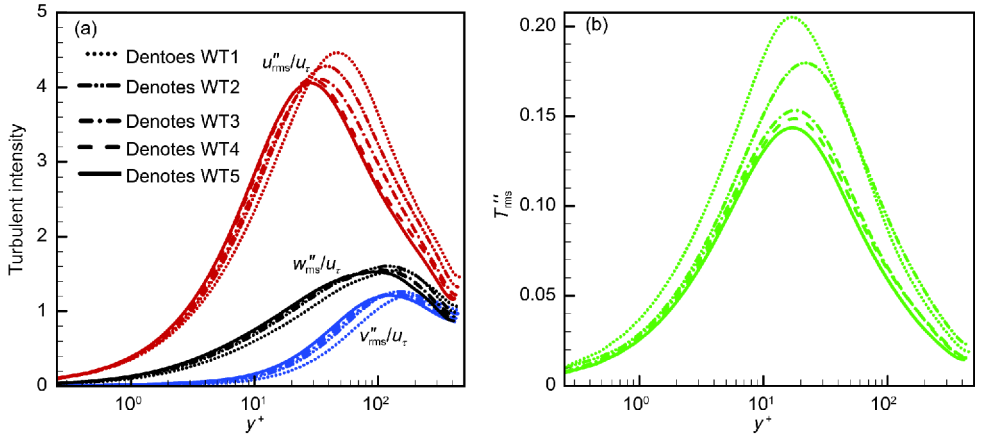

Figure 4 (Color online) Distributions of RMS velocity (a) and RMS temperature fluctuations (b) for different dimensional wall temperature.

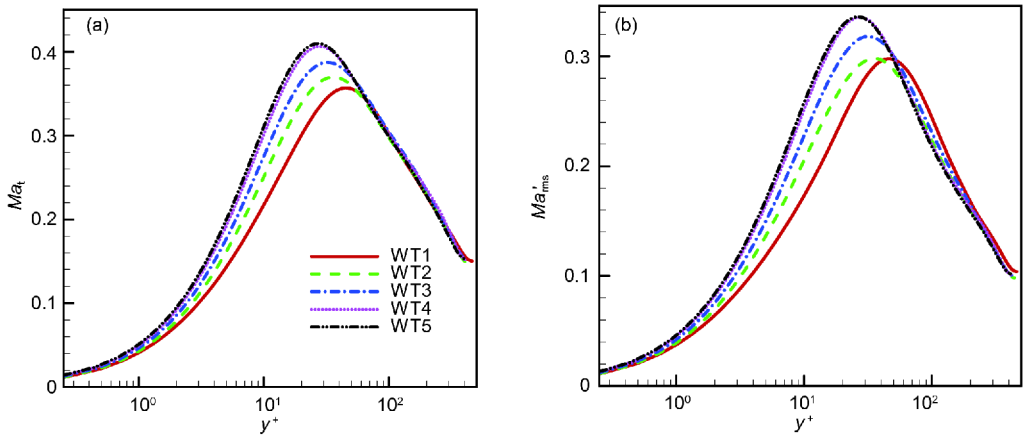

Figure 5 (Color online) Distributions of turbulent Mach number (a) and RMS Mach number fluctuation (b) for different dimensional wall temperature.

that the difference between Ma_t and Ma'_{rms} points to a significant non-zero VTC. We have examined the profiles of the relative deviation between Ma_t and Ma'_{rms}, and can confirm that analogous profiles exist for all cases, as shown in Figure 5(a) and (b). Moreover, the magnitude of Ma'_{rms} is smaller than that of Ma_t. It can be concluded that a significant VTC is observed.

Figure 6(a) and (b) show the probability density functions (PDFs) [19,50,51] of streamwise velocity fluctuation P_u and temperature fluctuation P_T near the wall ($1-|y|=0.04$), respectively. For comparison, the standard Gaussian distribution ($P_\alpha = \exp(-\alpha''^2/2)/\sqrt{2\pi}$, where α can be velocity, temperature, or another quantity) is also displayed. It should be emphasized that these PDFs are normalized to unit area. Note that the marginal PDFs are remarkably different from the standard Gaussian shape. Their tails are mostly shorter than that of a standard Gaussian. Since the left tails of P_u are shorter than the right tails, as shown in Figure 6(a), the high-order moments of the streamwise velocity fluctuation are determined by the right tails. With decreasing dimensional wall temperature, the left tails of P_u continue to overlap one another, whereas the right tails move apart. However, both the left and right tails of P_T overlap one another for different dimensional wall temperature, as shown in Figure 6(b). P_T departs only slightly from an almost symmetric standard Gaussian shape, and the profiles are shifted only slightly to the positive side of T'' for all cases.

Figure 7(a) and (b) show the PDF of streamwise velocity fluctuation with the associated sign of temperature fluctuation, P_u ($T''<0$, or $T''>0$), and the PDF of temperature fluctuation with the associated sign of the streamwise velocity fluctuation, P_T ($u''<0$, or $u''>0$), respectively. Note that the effects of the signs of u'' and T'' on the corresponding PDFs are similar. For example, P_u ($T''<0$) is almost completely confined to the negative side of T'', while the inverse trend is observed for P_u ($T''>0$). Since the right tail of P_u grows with increasing dimensional wall temperature, the influence of dimensional wall temperature is concentrated at P_u ($T''>0$).

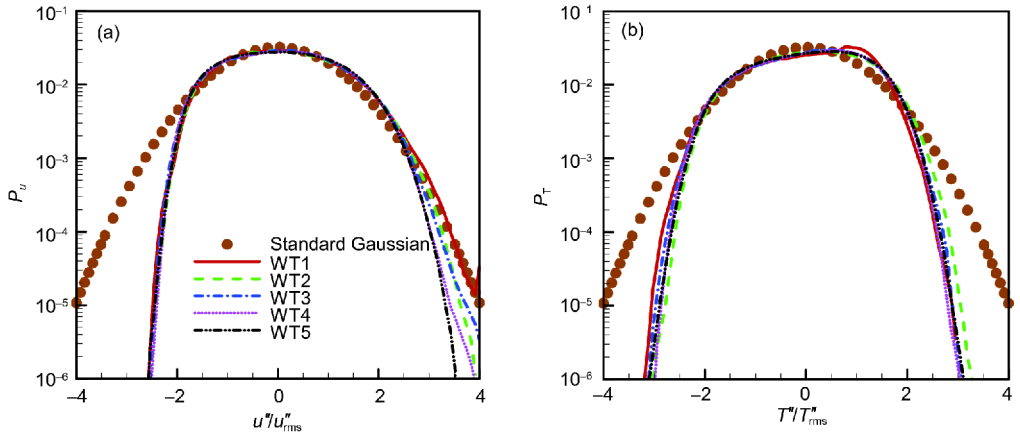

Figure 6 (Color online) PDFs of streamwise velocity fluctuation (a) and temperature fluctuation (b) near the wall ($1-|y|=0.04$) for different dimensional wall temperature.

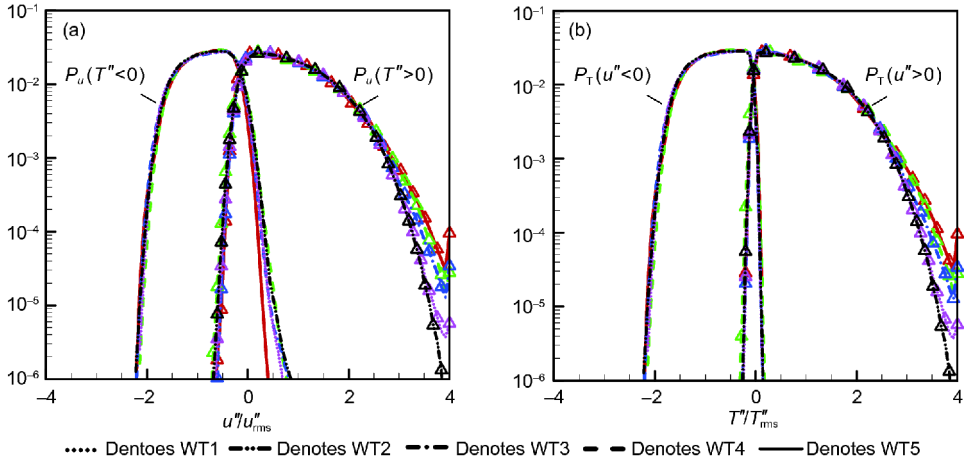

Figure 7 (Color online) PDFs of streamwise velocity fluctuation with the associated sign of temperature fluctuation (a) and temperature fluctuation with the associated sign of streamwise velocity fluctuation (b) near the wall ($1-|y|=0.04$) for different dimensional wall temperature.

4.2 Skin friction and heat transfer

The Stanton number C_h and skin friction coefficient C_f can be written as:

$$C_h = \frac{Q_w}{\rho_e u_e (h_{aw} - h_w)}, \quad C_f = \frac{\tau_w}{\frac{1}{2}\rho_e u_e^2}. \tag{18}$$

The mean VTC at the wall can be characterized by the Reynolds analogy ($C_h = 1/2C_f Pr^{-2/3}$), which can be quantified by the Reynolds analogy factor, defined by

$$R_{af} = \frac{2C_h}{C_f}. \tag{19}$$

Table 4 gives the skin friction C_f, Stanton number C_h and Reynolds analogy factor R_{af}. Note that C_f slightly increases and C_h slightly decreases with increasing dimensional wall temperature. R_{af} remains nearly constant and has a value of approximately 1.2 for all cases. These values are all within the range between 0.9 and 1.3, as reviewed by Roy and Blottner [52]. Therefore, the Reynolds analogy is still appropriate in this condition. In addition, the fluctuations in both τ_w and Q_w are close to 40% for all dimensional wall temperature cases, as shown in Table 4.

4.3 Walz's equation

Walz's equation [13] can be written as:

$$\frac{\{T\}}{T_w} = 1 + \frac{T_r - T_w}{T_w}\frac{\{u\}}{u_e} - r\frac{\gamma-1}{2}Ma_e^2\frac{T_e}{T_w}\left(\frac{\{u\}}{u_e}\right)^2, \tag{20a}$$

$$T_r = T_e\left(1 + r\frac{\gamma-1}{2}Ma_e^2\right), \tag{20b}$$

where T_r is the recovery temperature, r=0.89 is the recovery factor, and the subscript e indicates properties at the edge of the wall layer (the channel centerline in internal flow).

Table 4 Skin friction and heat transfer for different dimensional wall temperature

Cases	C_f ($\times 10^{-3}$)	C_h ($\times 10^{-3}$)	$2C_h/C_f$	Q'_{wrms}/Q_w	τ'_{wrms}/τ_w
WT1	7.128	4.401	1.234	0.401	0.389
WT2	7.156	4.294	1.200	0.407	0.385
WT3	7.197	4.247	1.180	0.401	0.391
WT4	7.281	4.208	1.156	0.409	0.399
WT5	7.208	4.199	1.165	0.410	0.402

Walz's equation improves the Crocco-Busemann relation and is in close agreement with the results of DNS for adiabatic compressible turbulent boundary layers, although it clearly deviates from DNS for isothermal supersonic turbulent boundary layers. Taking into account the wall heat flux q_w, Zhang et al. [26] have overcome the limitations of Walz's equation in the presence of nonadiabatic walls by introducing a general recovery factor,

$$\frac{\{T\}}{T_w} = 1 + \frac{T_{rg}-T_w}{T_w}\frac{\{u\}}{u_e} + \frac{T_e-T_{rg}}{T_w}\left(\frac{\{u\}}{u_e}\right)^2, \tag{21a}$$

$$\begin{aligned} T_{rg} &= T_e + r_g\frac{u_e^2}{2C_p}, \\ r_g &= 2(T_w-T_e)\frac{C_p}{u_e^2} - 2\mathrm{Pr}\frac{q_w}{u_e\tau_w}. \end{aligned} \tag{21b}$$

Modesti and Pirozzoli [53] found that eqs. (20) and (21) have the same form for external and internal flows. Figure 8(a) provides a comparison between the DNS data and the predictions of eqs. (20) and (21) for WT5. Note that eq. (21) gives better results. Similar results have been observed for calorically perfect gas [53]. The VTC predicted by the eq. (21) does not differ much from that obtained from DNS data, as shown in Figure 8(b). Moreover, the curvature of the quadratic function decreases with increasing dimensional wall temperature.

To remove the explicit dependence of the velocity-temperature relation on thermal and chemical models, Duan and Martín [27] introduced a nondimensional "recovery enthalpy",

$$h_r^* = \frac{\{h_r\}-h_w}{h_e-h_w}, \tag{22a}$$

$$\{h_r\} = \{h\} + r\frac{\{u\}^2}{2}, \tag{22b}$$

$$\frac{\{h\}}{h_e} = \frac{h_w}{h_e} + \frac{h_e-h_w}{h_e}f\left(\frac{\{u\}}{u_e}\right) - r\frac{\frac{1}{2}u_e^2}{h_e}\left(\frac{\{u\}}{u_e}\right)^2, \tag{22c}$$

where $f(\{u\}/u_e)$ is nearly independent of free stream Mach number, wall temperature, surface catalysis and enthalpy conditions and can be fitted to a curve of the form

$$f\left(\frac{\{u\}}{u_e}\right) = 0.1741\left(\frac{\{u\}}{u_e}\right)^2 + 0.08259\left(\frac{\{u\}}{u_e}\right). \tag{23}$$

Figure 9 shows the nondimensional "recovery enthalpy" h_r^*. It can be seen that h_r^* collapses the profiles for different dimensional wall temperature.

4.4 Strong Reynolds analogy

Morkovin [9] proposed a number of SRA relations, three of which are listed below:

$$\frac{T'_{rms}/\{T\}}{(\gamma-1)Ma^2\left(u'_{rms}/\{u\}\right)} \approx 1, \tag{24}$$

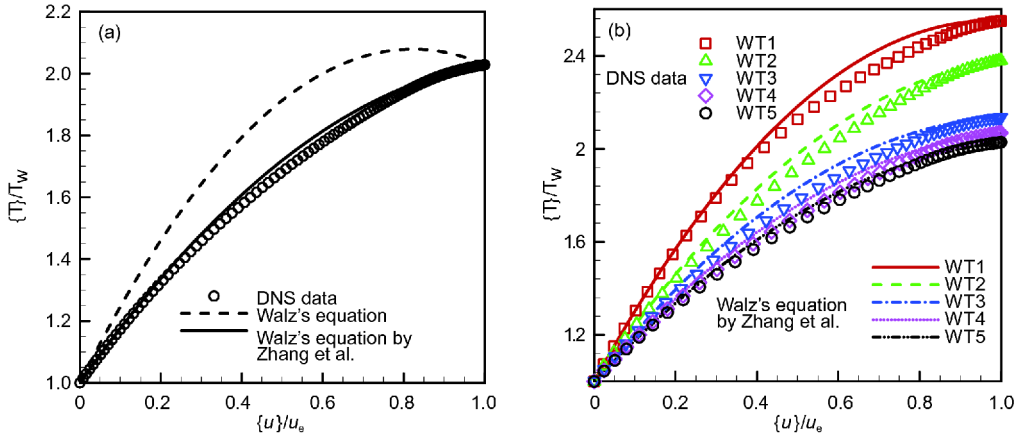

Figure 8 (Color online) Relationship between mean temperature and mean streamwise velocity for WT5 (a) and different dimensional wall temperature (b).

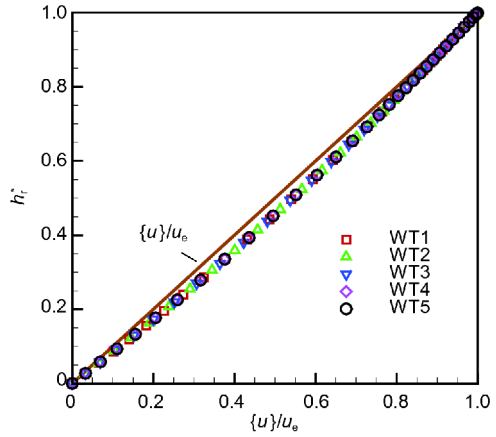

Figure 9 (Color online) Distribution of "Recovery enthalpy" h_r^* versus mean streamwise $\{u\}/u_e$ for different dimensional wall temperature.

$$R_{u''T''} = \frac{\langle u''T''\rangle}{u''_{\rm rms}T''_{\rm rms}} \approx 1, \tag{25}$$

$$Pr_{\rm t} = \frac{\langle \rho u''v''\rangle(\partial\{T\}/\partial y)}{\langle \rho v''T''\rangle(\partial\{u\}/\partial y)} \approx 1, \tag{26}$$

where $Pr_{\rm t}$ is called the turbulent Prandtl number and is a measure of the ratio of the turbulent kinematic heat transfer to the turbulent kinematic momentum transfer.

Several "modified" forms of SRA have been proposed to account for the heat flux at the wall and remove its wall temperature dependence. For example, Cebeci and Smith [32] derived an extended SRA (ESRA) based on eq. (24)

$$\frac{T'_{\rm rms}/\{T\}}{(\gamma-1)Ma^2\left(u'_{\rm rms}/\{u\}\right)} \approx \left|1 + C_{\rm p}\frac{\{T_{\rm w}\}-\{T_{{\rm t},c}\}}{\{u\}\{u_c\}}\right|, \tag{27}$$

where $T_{\rm t}$ denotes the total temperature.

Gaviglio [29], Rubesin [33] and Huang et al. [30] have also proposed modified SRA relations, denoted as GSRA, RSRA and HSRA, which correspond to $c = 1.0$, $c = 1.34$, and $c = Pr_{\rm t}$, respectively, in the following equation:

$$\frac{T''_{\rm rms}/\{T\}}{(\gamma-1)Ma^2(u''_{\rm rms}/\{u\})} \approx \frac{1}{c[1-\partial\{T_T\}/\partial\{T\}]}. \tag{28}$$

More recently, by removing the assumption of calorically perfect gas, Duan and Martín [27] derived the following extended form of the HSRA (GHSRA) as below:

$$T''_{\rm rms} = -\frac{1}{Pr_{\rm t}}\frac{\partial\{T\}}{\partial\{u\}}u''_{\rm rms}. \tag{29}$$

Figure 10 shows the results of SRA and the modified SRAs for different dimensional wall temperature. As can be seen from Figure 10(a) and (b), SRA and ESRA give results that are inconsistent with observations. Similar results for calorically perfect gas have been reported by Gaviglio [29]. As explained by Morinishi et al. [37], not only is the total temperature fluctuation not negligible compared with the

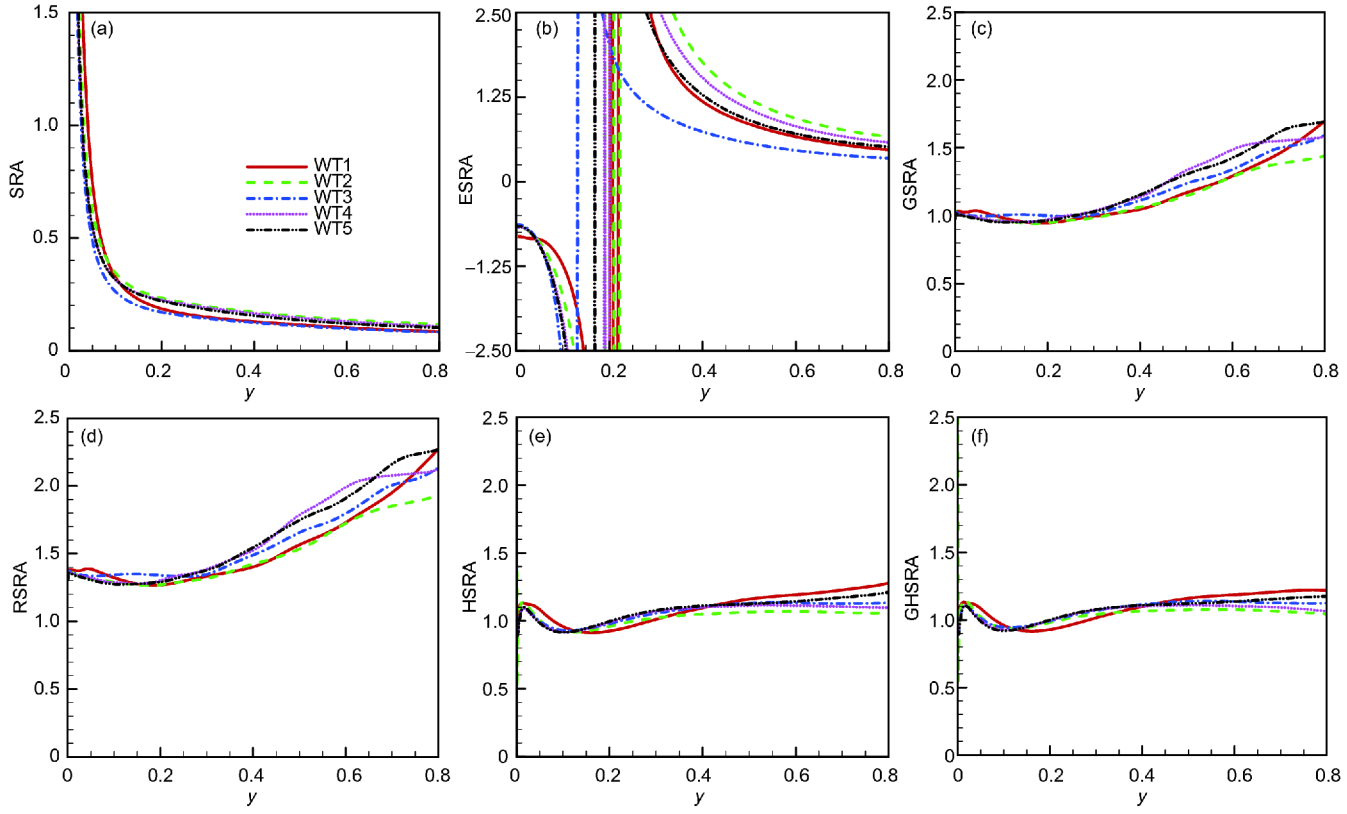

Figure 10 (Color online) Distributions of SRA (a), ESRA (b), GSRA (c), RSRA (d), HSRA (e) and GHSRA (f) for different dimensional wall temperature.

temperature fluctuation, but also the condition of $\langle T''^2\rangle / \{T\}^2 \ll \left(\langle T''^2_T\rangle - 2\langle T''T''_T\rangle / \{T\}^2\right)$ is not satisfied. The trend exhibited by the GSRA is the same as that of the RSRA, and the magnitude of GSRA is closer to 1 than that for RSRA, as shown in Figure 10(c) and (d). The values of the HSRA and GHSRA remain close to 1 among the channel, as shown in Figure 10(e) and (f). Therefore, HSRA and GHSRA are better than other modified SRAs at predicting results for STCF of TPG. In addition, both the original SRA and its modified SRA versions are relatively insensitive to dimensional wall temperature.

Figure 11(a) shows the correlation coefficient between streamwise velocity and temperature fluctuation $R_{u''T''}$, as expressed in eq. (25). Note that $R_{u''T''}$ is positive among the channel, which indicates that u'' and T'' are positively correlation, i.e., low streamwise velocities are associated with low temperatures, and large streamwise velocities are associated with high temperatures. This phenomenon, oriented from quadrants 1 to 3, can also be observed in the instantaneous joint probability density (JPD) of streamwise velocity fluctuation versus temperature fluctuation near the wall ($1-|y|=0.04$) for WT5, as shown in Figure 11(b). According to the gradient diffusion hypothesis [10], positive u'' transports hot gas to a colder region, which results in a positive T''. $R_{u''T''}$ near to unity close the wall, but decreases rapidly moving away from the wall. This behavior is similar to that found for calorically perfect gas by Coleman et al. [35] and Morinishi et al. [37]. Moreover, $R_{u''T''}$ is insensitive to the dimensional wall temperature.

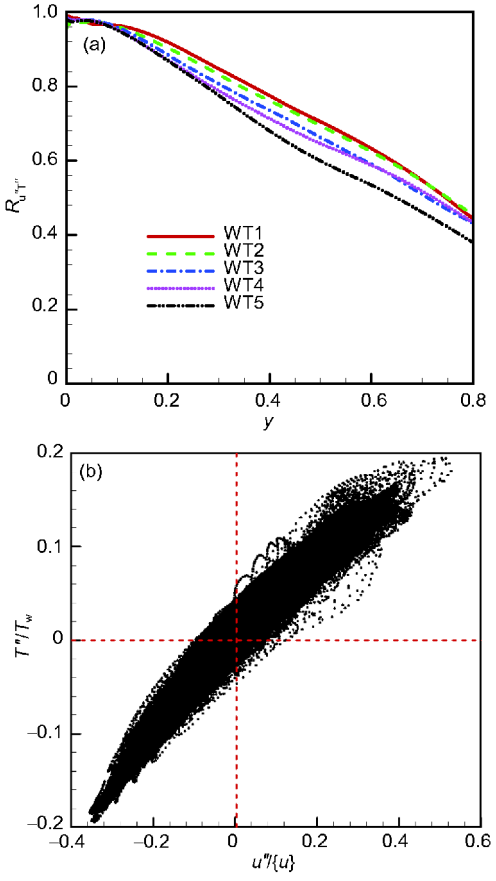

Figure 11 (Color online) (a) Distribution of $R_{u''T''}$ for different dimensional wall temperature; (b) joint probability density of instantaneous streamwise velocity fluctuation versus temperature fluctuation near the wall ($1-|y|=0.04$) for WT5.

Figure 12 shows the turbulent Prandtl number Pr_t, as expressed in eq. (26). It can be seen that Pr_t is relatively insensitive to the dimensional wall temperature, and remains close to unity among the channel.

5 Conclusions

Based on the assumption of TPG, we have performed DNS of STCFs with Mach number 3.0 and Reynolds number 4880 to study the influence of dimensional wall temperature on VTC. The dimensional wall temperature ranges from 298.15 to 1192.60 K. For dimensional wall temperature up to 596.30 K, the vibrational energy is important, since the vibrational energy excited degree is greater than 0.1.

The van Driest transferred mean velocity collapse for different dimensional wall temperature with incompressible flows. The mean and fluctuating temperature decrease with increasing dimensional wall temperature. The difference between turbulent Mach number and RMS Mach number fluctuation leads to significantly non-zero VTC. The tails of the PDFs of streamwise velocity and temperature fluctuations are shorter than that of a standard Gaussian. The influence of dimensional wall temperature is greatest on the right tails of the PDF of streamwise velocity fluctuation, and increases with increasing dimensional wall temperature. The Reynolds analogy factor remains close to 1.2 for all dimensional wall temperature cases.

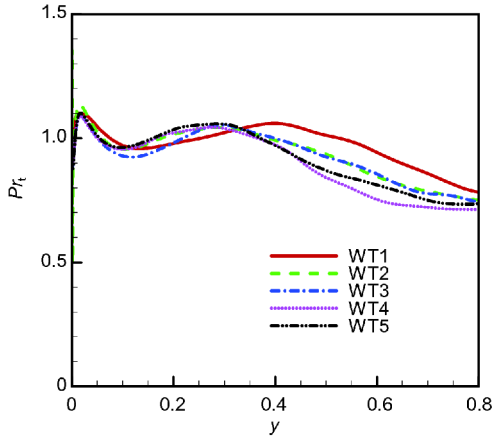

Figure 12 (Color online) Distribution of Pr_t for different dimensional wall temperature.

The mean temperature is a quadratic function of the mean velocity. The profiles do not collapse and their curvatures increase with increasing dimensional wall temperature. Walz's equation gives poorer results than the modification by Zhang et al. The introduction of "recovery enthalpy" provides an explanation of the relation between mean velocity and mean temperature, which is independent of dimensional wall temperature.

SRA is relatively insensitive to the dimensional wall temperature among the channel, although the original SRA relation breaks down for all dimensional wall temperature cases. The modifications of SRA by Huang et al. [30] and Zhang et al. [26] provide reasonably good results and are better than the modifications by Cebeci and Smith and by Rubesin. The streamwise velocity and temperature fluctuations are perfectly anticorrelated and the turbulent Prandtl number is close to unity.

This work was supported by the National Natural Science Foundation of China (Grant Nos. 11502236, 51536008, and 91852203), the National Key Research and Development Program of China (Grant No. 2016YFA0401200), Science Challenge Project (Grant No. TZ2016001), and the Natural Science Foundation of Zhejiang Province (Grant No. LQ16E090005).

1 L. Fulachier, F. Anselmet, R. Borghi, and P. Paranthoen, J. Fluid Mech. **203**, 577 (1989).
2 C. Brun, M. Petrovan Boiarciuc, M. Haberkorn, and P. Comte, Theor. Comput. Fluid Dyn. **22**, 189 (2008).
3 P. Bradshaw, Annu. Rev. Fluid Mech. **9**, 33 (1977).
4 S. K. Lele, Annu. Rev. Fluid Mech. **26**, 211 (1994).
5 H. Schlichting, *Boundary-layer theory 3rd* (McGraw-Hill, New York, 1968).
6 E. F. Spina, A. J. Smits, and S. K. Robinson, Annu. Rev. Fluid Mech. **26**, 287 (1994).
7 A. Busemann, *In: Leipzig Geest, Portig* (Handbuch der physik, 1931).
8 L. Crocco, L'Aerotecnica **12**, 181 (1932).
9 M. V. Morkovin, *Mécanique de la Turbulence* (CNRS, Metz, 1961), p. 367.
10 A. J. Smits, and J. P. Dussauge, *Turbulent Shear Layers in Supersonic Flow* (Springer, Berlin, 2006).
11 O. Reynolds, Int. J. Heat Mass Transfer **3**, 163 (1961).
12 E. R. van Driest, J. Spacecraft Rockets **40**, 1012 (2003).
13 A. Walz, *Boundary Layers of Flow and Temperature* (MIT Press, Cambridge, 1969).
14 D. L. Whitfield, and M. D. High, AIAA J. **15**, 431 (1977).
15 A. J. Laderman, and A. Demetriades, J. Fluid Mech. **63**, 121 (1974).
16 A. J. Laderman, AIAA J. **16**, 723 (1978).
17 F. K. Owen, C. C. Horstman, and M. I. Kussoy, J. Fluid Mech. **70**, 393 (1975).
18 M. J. Tummers, E. H. van Veen, N. George, R. Rodink, and K. Hanjalić, Exp. Fluid **37**, 364 (2004).
19 L. Pietri, M. Amielh, and F. Anselmet, Int. J. Heat Fluid Flow **21**, 22 (2000).
20 Y. Q. Wang, and C. Q. Liu, Sci. China-Phys. Mech. Astron. **60**, 114712 (2017).
21 T. B. Gatski, and J. P. Bonnet, *Compressibility, Turbulence and High Speed Flow* (Elsevier, Amsterdam, 2009).
22 S. Pirozzoli, F. Grasso, and T. B. Gatski, Phys. Fluid **16**, 530 (2004).
23 T. Maeder, N. A. Adams, and L. Kleiser, J. Fluid Mech. **429**, 187 (2001).
24 L. Duan, I. Beekman, and M. P. Martín, J. Fluid Mech. **655**, 419 (2010).
25 L. Duan, I. Beekman, and M. P. Martín, J. Fluid Mech. **672**, 245 (2011).
26 Y. S. Zhang, W. T. Bi, F. Hussain, and Z. S. She, J. Fluid Mech. **739**, 392 (2014).
27 L. Duan, and M. P. Martín, J. Fluid Mech. **684**, 25 (2011).
28 S. E. Guarini, R. D. Moser, K. Shariff, and A. Wray, J. Fluid Mech. **414**, 1 (2000).
29 J. Gaviglio, Int. J. Heat Mass Transfer **30**, 911 (1987).
30 P. G. Huang, G. N. Coleman, and P. Bradshaw, J. Fluid Mech. **305**, 185 (1995).
31 R. Lechner, J. Sesterhenn, and R. Friedrich, J. Turbul. **2**, N1 (2001).
32 T. Cebeci, and A. M. O. Smith, *Analysis of Turbulent Boundary Layers* (Academic Press, New York, 1974).
33 M. W. Rubesin, *Extra Compressibility Terms for Favre-Averaged Two-Equation Models of Inhomogeneous Turbulent Flows*, Technical Report (NASA, 1990).
34 X. Liang, and X. L. Li, Sci. China-Phys. Mech. Astron. **56**, 1408 (2013).
35 G. N. Coleman, J. Kim, and R. D. Moser, J. Fluid Mech. **305**, 159 (1995).
36 S. Tamano, and Y. Morinishi, J. Fluid Mech. **548**, 361 (2006).
37 Y. Morinishi, S. Tamano, and K. Nakabayashi, J. Fluid Mech. **502**, 273 (2004).
38 J. D. Anderson, *Hypersonic and High Temperature Gas Dynamics* (AIAA, New York, 2000).
39 O. Marxen, T. Magin, G. Iaccarino, and E. S. G. Shaqfeh, Hypersonic boundary-layer instability with chemical reactions, AIAA Paper 2010-0707, 2010.
40 W. Jia, and W. Cao, Appl. Math. Mech.-Engl. Ed. **31**, 979 (2010).
41 X. P. Chen, X. P. Li, H.-S. Dou, and Z. C. Zhu, Sci. Sin.-Phys. Mech. Astron. **41**, 969 (2011).
42 X. Chen, X. Li, H. S. Dou, and Z. Zhu, J. Turbul. **19**, 365 (2018).
43 Z. Chen, C. P. Yu, L. Li, and X. L. Li, Sci. China-Phys. Mech. Astron. **59**, 664702 (2016).
44 Y. C. Hu, W. T. Bi, S. Y. Li, and Z. S. She, Sci. China-Phys. Mech. Astron. **60**, 124711 (2017).
45 X. L. Li, D. X. Fu, Y. W. Ma, and X. Liang, Sci. China-Phys. Mech. Astron. **53**, 1651 (2010).
46 X. Li, D. Fu, and Y. Ma, AIAA J. **46**, 2899 (2008).
47 X. Li, D. Fu, and Y. Ma, Phys. Fluids **22**, 025105 (2010).
48 G. S. Jiang, and C. W. Shu, J. Comput. Phys. **126**, 202 (1996).
49 J. Fan, Chin. J. Theor. Appl. Mech. **42**, 591 (2010) (in Chinese).
50 S. B. Pope, *Turbulence Flow* (Cambridge University Press, Cambridge, 2001).
51 J. Wang, T. Gotoh, and T. Watanabe, Phys. Rev. Fluids **2**, 053401 (2017).
52 C. J. Roy, and F. G. Blottner, Prog. Aerospace Sci. **42**, 469 (2006).
53 D. Modesti, and S. Pirozzoli, Int. J. Heat Fluid Flow **59**, 33 (2016).